Supporting information:

Sequential electrostatic assembly of a polymer surfactant corona increases activity of the phosphotriesterase arPTE.

William H. Zhang[1], Benjamin M. Carter[1], Graham Day[1], Norman Govan[2], Colin Jackson[3*], Adam Perriman[1*]

[1]University of Bristol, School of Cellular and Molecular Medicine. BS8 1TD, United Kingdom.

[2]Defence Science and Technology Laboratory. SP4 0JQ, United Kingdom.

[3]Australian National University, Research School of Chemistry. ACT 2601, Australia.

*chawp@bristol.ac.uk; *cjackson@rsc.anu.edu.au

Table of contents

1. Methods

Expression of enzymes

With the exception of arPTE (PETMCS1), all genes were encoded in the PETMCS3 vector (with HIS-Tag). All genes were transformed into BL21(DE3) *E. coli* cells and were expressed without chemical induction. arPTE and pdPTE-C23 were grown in Terrific Broth (TB; Fisher, UK) supplemented with 100 µM cobalt chloride and 50 mg carbenicillin at 25 °C for 36-48 hours. DFPase was grown in the same manner, but without cobalt chloride supplementation. αEst7 was grown in LB media supplemented with 50 mg carbenicillin for 16 hours. All cells were harvested through centrifugation and either purified immediately or the pellets were stored at -20 °C for future purification.

Purification of arPTE

A bacterial cell pellet (from 500 mL of culture) was resuspended in 25 mL of buffer (30 mM HEPES, 100 µM cobalt chloride, pH 8.0) and lysed through sonication. The lysate was clarified through high-speed centrifugation and the supernatant was retained. The supernatant was loaded onto a DEAE–Sepharose column (GE Healthcare, UK) that had been pre-equilibrated with buffer (30 mM HEPES, 100 µM cobalt chloride, pH 8.0) and the column underwent isocratic elution with the same buffer. The fractions containing arPTE were pooled and then concentrated into a small volume (5-10 mL), which was then loaded onto a pre-equilibrated Superdex 200 pg HiLoad 26/600 column (GE Healthcare) and underwent isocratic elution with buffer (30 mM HEPES, 100 µM cobalt chloride, pH 8.0). The peak fractions from the size exclusion chromatography (SEC) purification were pooled and was stored at 4 °C for future use. The protein after SEC had single band purity as assessed by SDS page electrophoresis.

Purification of his-tagged enzymes

A bacterial cell pellet (from 1 L of culture for pdPTE-C23 and DFPase, 6 L for αEst7) was resuspended in 30 mL of buffer (30 mM HEPES, 200 mM NaCl, 20 mM imidazole, pH 8.0) and lysed through sonication. The lysate was clarified through high-speed centrifugation and the supernatant was retained. The supernatant was loaded onto either a nickel affinity column (HisTrap FF, GE Healthcare, UK) for DFPase and αEst7, or a cobalt affinity column (HisPur, Thermoscientific, UK) for pdPTE-C23 and his-arPTE, and washed with 10–15x column volumes of buffer (30 mM HEPES, 200 mM NaCl, 20 mM imidazole, pH 8.0). The protein was then eluted with buffer (30 mM HEPES, 200 mM NaCl, 250 mM imidazole, pH 8.0) and the fractions containing the protein were retained. The protein was concentrated into a small volume (5–10 mL), which was then loaded onto a pre-equilibrated Superdex 200 pg HiLoad 26/600 column (GE Healthcare) and underwent isocratic elution with an appropriate buffer (30 mM HEPES, 100 µM cobalt chloride, pH 8.0 for pdPTE-C23; 30 mM HEPES, 100 µM calcium chloride, pH 8.0 for DFPase; 30 mM HEPES, 200 mM sodium chloride, pH 8.0 for αEst7). The peak fractions from the SEC purification were pooled and was stored at 4°C for future use. The proteins after SEC had single band purity as assessed by SDS page electrophoresis. The presence of a his-tag does not appear to influence the rate enhancement of the surfactant corona, as confirmed by assaying his-tagged arPTE and the corresponding surfactant complex (**Figure S9**).

Synthesis of oxidized IGEPAL-890

The method for IGEPAL-890 oxidation was followed as previously described by Armstrong *et al.*(*1*) In brief, IGEPAL-890 (2 g, 1.0 mmol) was dissolved in MilliQ water (50 mL), and Sodium Bromide (50 mg, 0.49 mmol), Sodium Hypochlorite (5 mL, 10–15% available chlorine) and TEMPO (30 mg, 0.19 mmol) was then added to the stirring solution. The solution was basified to pH 11.0 and allowed to stir overnight, after which, the solution was acidified to pH 1.0 and extracted 3 times with chloroform (80 mL each). The chloroform was then washed 3 times with pH 1.0 MilliQ water (80 mL each) and then the chloroform was removed by rotary evaporation. The resulting oil was further purified through recrystallization in neat ethanol at -20 °C.

Enzyme conjugation procedure

The amount of surfactant used for conjugation was determined using the following formula:

$$\text{Moles of surfactant} = \text{Moles of enzyme} \times \text{number of charged residues} \times 2$$

With the number of charged residues being the number of anionic residues for the cationic surfactant, and the number of cationic residues for the anionic surfactant. The cationic surfactant (Ethoquad) was dissolved in the same buffer as the corresponding enzyme and then rapidly added to a stirring solution of enzyme (100–150 µM). The solution was stirred for 3 hours at which point a solution containing anionic surfactant (Usually oxidized IGEPAL-890), which was prepared in an identical manner to the cationic surfactant, was added and the resulting solution allowed to stir for 3 hours or overnight. The solution then underwent dialysis with MilliQ water for 16–24 hours with one change of the external dialysis solution at 3 hours.

The stoichiometry of the sample was determined by comparing the absorbance of the enzyme complex to a sample of uncmodified enzyme at an equivalent concentration. The difference in absorbance was taken and used to calculate the molar equivalents of oxidized IGEPAL-CO890 using the extinction coefficient of 1563 $L \cdot M^{-1} \cdot cm^{-1}$. The Ethoquad was assumed to be complexed at a comparable stoichiometry. A typical ratio of charged residues to surfactant molecules is between 1:1.2 to 1:1.3.

SR-SAXS sample preparation and analysis

The data for the enzyme bioconjugates ([arPTE][S^+][S^-], [pdPTE-C23][S^+][S^-], [αEst7][S^+][S^-], and [DFPase][S^+][S^-]) was obtained using synchrotron radiation small angle X-ray scattering (SR-SAXS) on the I22 beamline at the Diamond Light Source, Oxford. For all unmodified enzymes, including the data used to generate the bead model for arPTE, the data was obtained using the B21 beamline mail-in service, using the size exclusion chromatography option (SEC-SR-SAXS). Prior to sample submission or analysis, samples were concentrated with 10K MWCO spin concentrators and flowthrough retained for use as backgrounds. The samples were then spun through 1 million MWCO spin concentrators to remove large contaminants. All samples were at analysed at 1-2 mg/ml concentration. For the I22 beamline, samples were loaded into 100 µm capillary tubes and 1 frame was recorded for 1 second. Data preparation and reduction to generate the 2D scattering profiles were performed using DAWN.(*2*) Both the Porod exponent and the pair-distance distribution function (P(r)) for a given enzyme were determined using the ScÅtter software package with ATSAS plugins,(*3, 4*) following the procedure as described in the tutorial. Further to this, the radius of gyration ($R_{g,}$ real space), radial average (r_{ave}), and maximum diameter (d_{max}) were derived from the P(r). The DAMMIF plugin was used in scatter to generate the bead-models of arPTE and [arPTE][S^+][S^-] from the respective P(r).

Assay conditions for paraoxon-ethyl (arPTE, pdPTE-C23, αEst7)

The hydrolysis of paraoxon-ethyl to produce 4-nitrophenol was monitored at 405 nM using a plate reader (BioTek Synergy Neo 2). A given assay used 2-10 nM of enzyme and was performed in the same buffer that the enzyme was stored in, with or without BSA as necessary. Dilutions of the enzyme used buffer already containing the appropriate agents (BSA) ensuring that the enzyme would not require equilibration time with these agents when assayed. All assays were performed at room temperature.

Assay conditions for diisopropyl fluorophosphate (DFPase)

Assays were performed using a fluoride selective probe (SciQuip) monitoring the conductivity change over time. The probe was calibrated, and a standard curve developed, using a fluoride standard (SciQuip). Assays used 500 nM of enzyme and were performed in 30 mM HEPES, 100 µM calcium chloride, pH 8.0 at room temperature. The enzyme was equilibrated with the buffer for 3 minutes with constant stirring, after which the reaction was initiated by the addition of diisopropyl fluorophosphate (DFP, in isopropanol to aid solubility).

Statistical and data analysis

Data and statistical analysis, as well as Michaelis–Menten parameters were determined using Graphpad Prism. To further elucidate the mechanism of rate enhancement, the data was fit to the model described by Breger *et al.*(*5*) that separates the k_1 and k_2 contributions to k_{obs}. Non-linear regression was performed while fixing either k_1 or k_2 using the SciPy Python package.

2. Supplementary figures

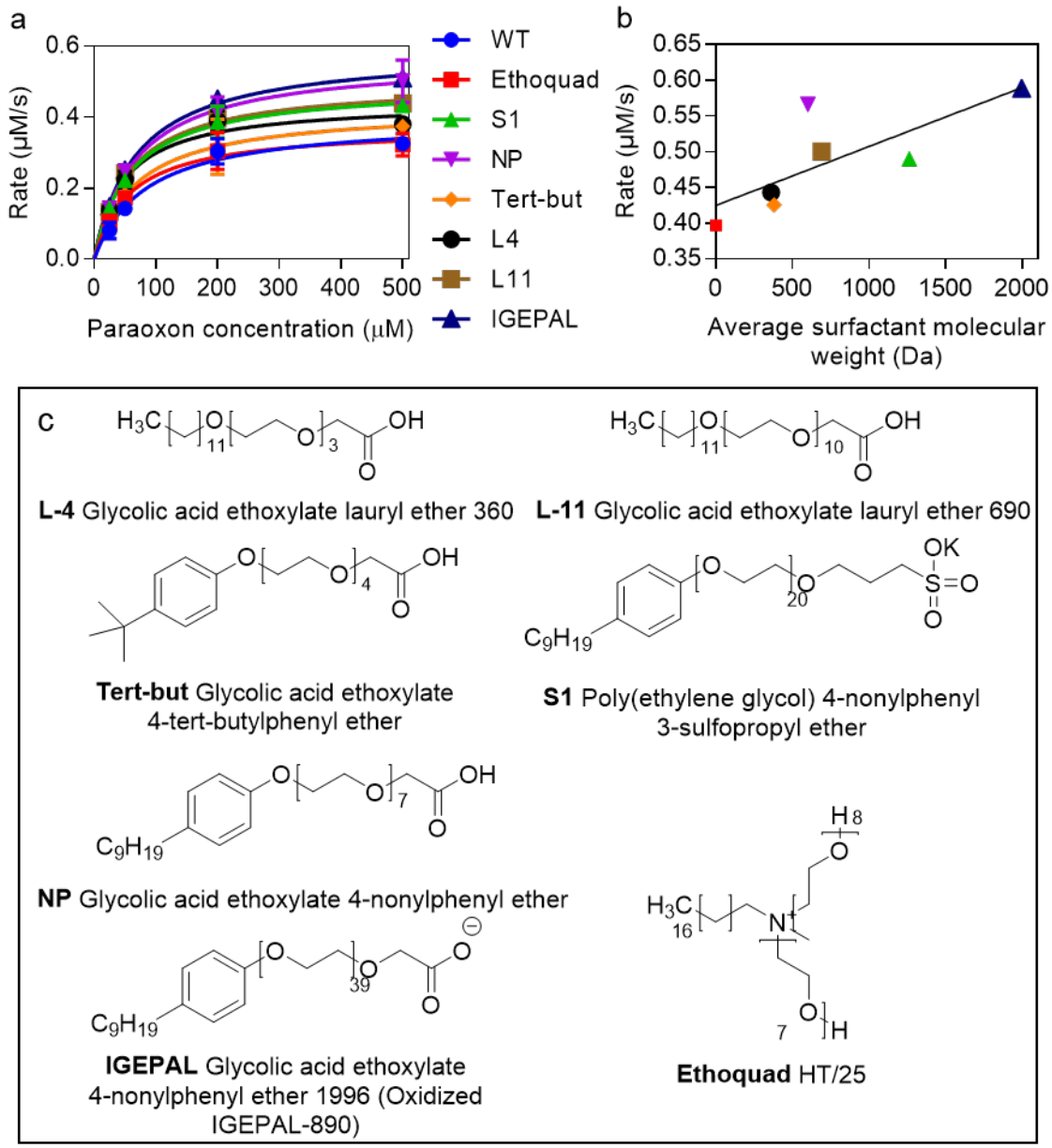

Figure S1: a) The enzyme arPTE was assayed without surfactants (WT, blue circle), with only the cationic surfactant (Ethoquad, red square), and then with the combination of Ethoquad and an anionic surfactant (S1, green triangle, NP, purple inverted triangle, Tert-but, orange diamond, L4, black circle, L11, brown, IGEPAL-890, dark blue triangle). Ethoquad and the unmodified enzyme did not have a significant difference in k_{cat}. The single addition of Ethoquad did not have any significant affect on the observed rate or affinity, same batch arPTE vs [arPTE][S^+] k_{cat} = 265 ± 16 s^{-1} vs 248 ± 16 $s^{-}1$, Km = 56 ± 10 μM vs 58 ± 13 μM. b) Analysis of the correlation between surfactant size (excluding the Ethoquad mass) and the observed k_{cat} demonstrating a positive correlation between surfactant size and the catalytic rate of the enzyme. Pearson r 0.776, $P < 0.05$. The colour legend is the same as described in Figure S1a. c) The chemical structures of the surfactants used in this study.

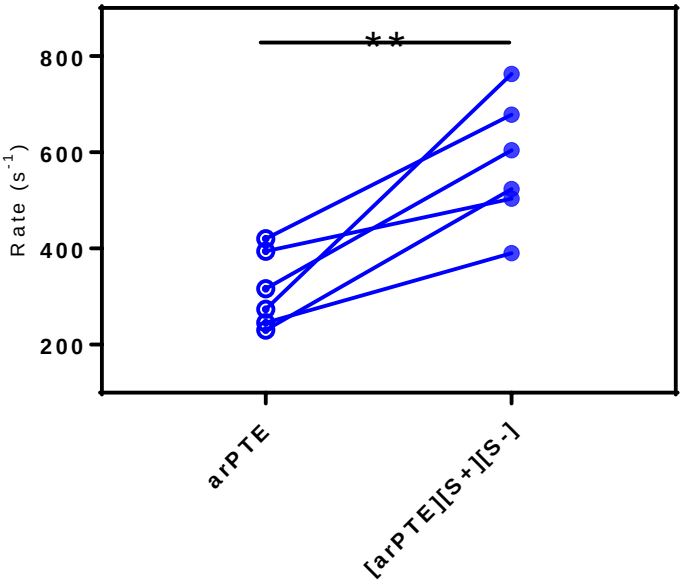

Figure S2: Rate variability (k_{cat}) between different batches/purifications of enzyme with same-batch unmodified (arPTE) and complexed ([arPTE][S^+][S^-]) enzyme paired together (paired t-test, $P < 0.01$)**.** In all cases there is an increase in activity after conjugation.

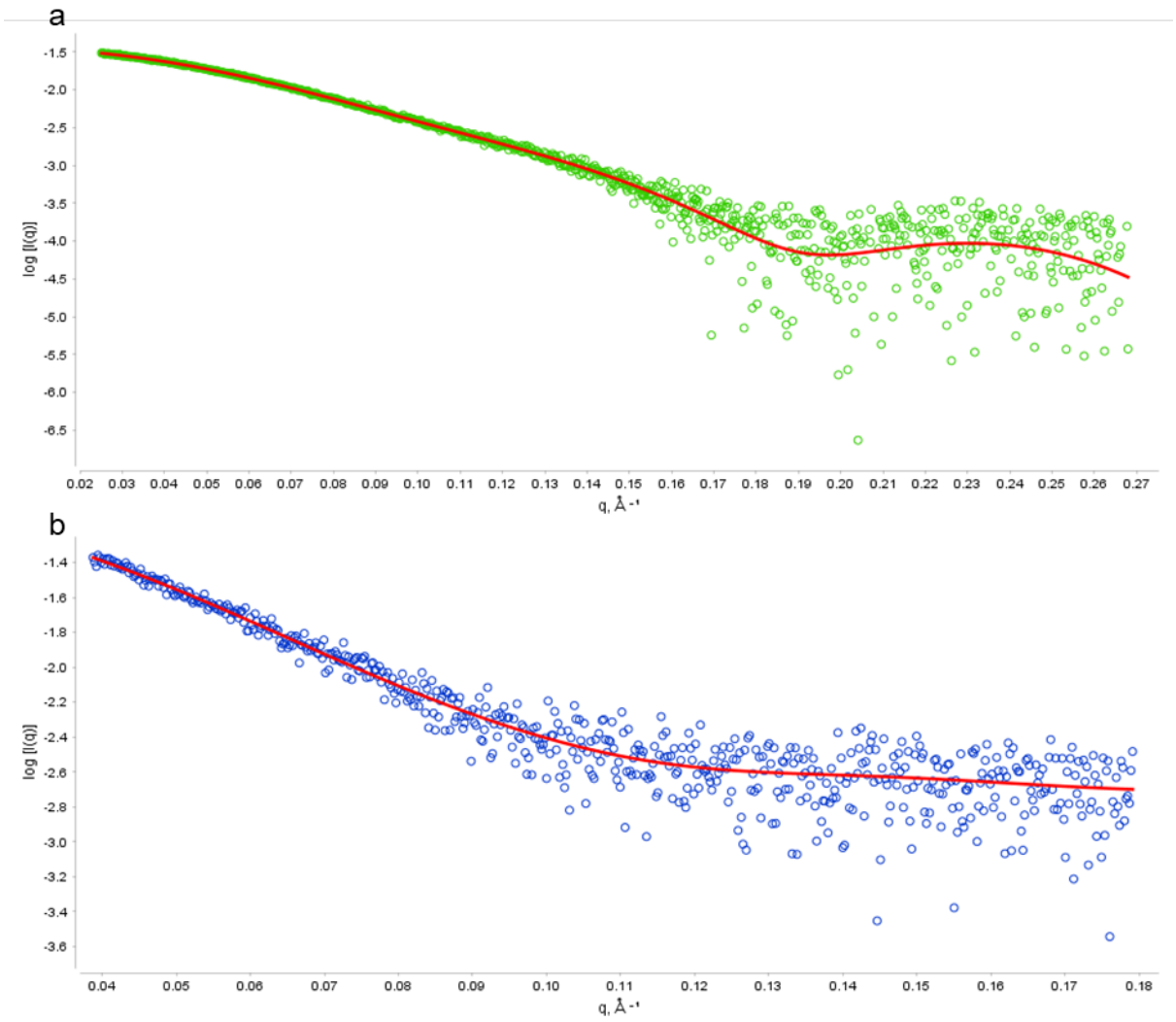

Figure S3: The scattering intensity plots (log) of a) arPTE and b) [arPTE][S^+][S^-] analysed through SR-SAXS as described in the methods. The fits from the ScÅtter software package analysis (red line) are shown and were used to create the bead-models. The arPTE data was obtained using the B21 mail-in service (SEC-SAXS), while the [arPTE][S^+][S^-] data was obtained from the I22 beamline.

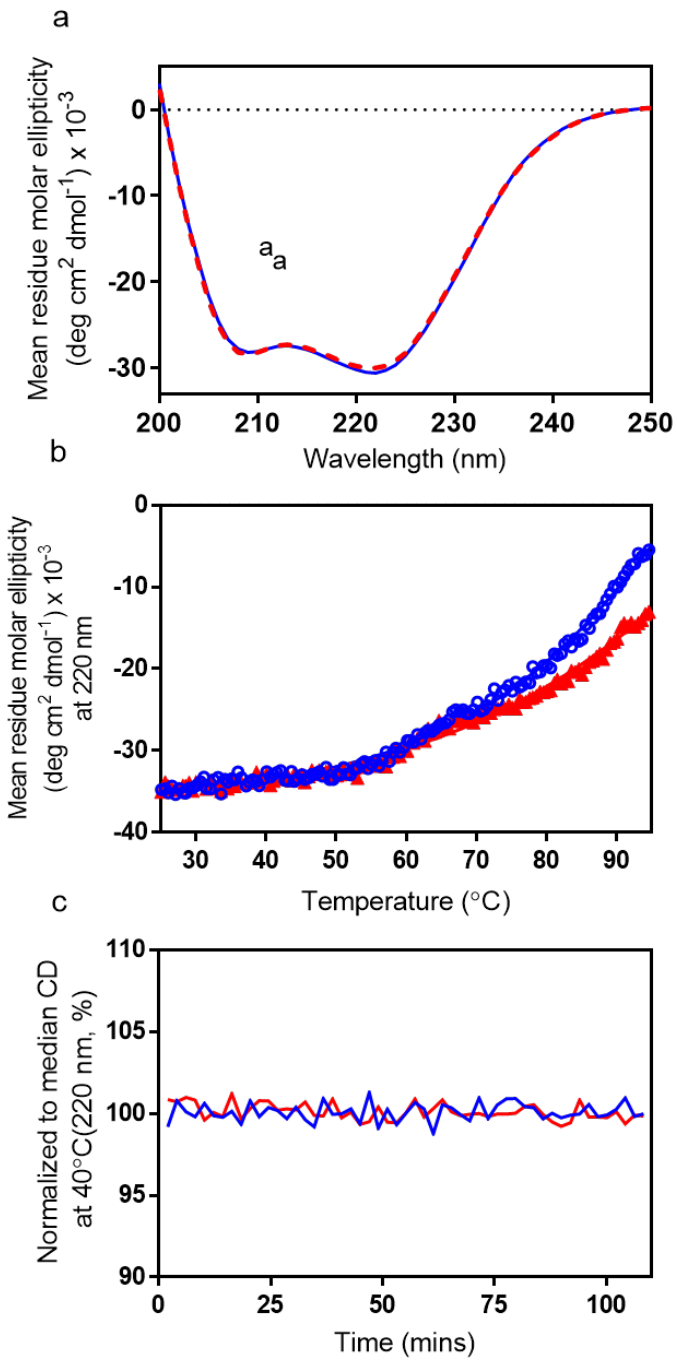

Figure S4: a) A superimposition of the CD spectra of arPTE (blue) and [arPTE][S^+][S^-] (dashed red lines) showing that the structural integrity of the enzyme remains intact after conjugation, and that there are no significant changes to the secondary structure of the enzyme as a result of the conjugation. arPTE and [arPTE][S^+][S^-] were diluted from a concentrated stock of the enzyme in buffer (30 mM HEPES, 100 µM cobalt chloride, pH 8.0) into MilliQ water to a concentration of 2.7 µM. The sample was recorded at 25°C with a 1 mm pathlength cuvette. b) A temperature gradient of arPTE vs [arPTE][S^+][S^-] at 220 nm from 25 °C to 95 °C shows slightly elevated thermostability of [arPTE][S^+][S^-] (81.3 ± 0.2 vs 87.7 ± 0.3 respectively, single sigmoid model). c) A time course study of arPTE (blue) and arPTE][S^+][S^-] (red) at 40°C showing that even at elevated temperatures there is no structural denaturation of the enzyme (monitored at 220 nm).

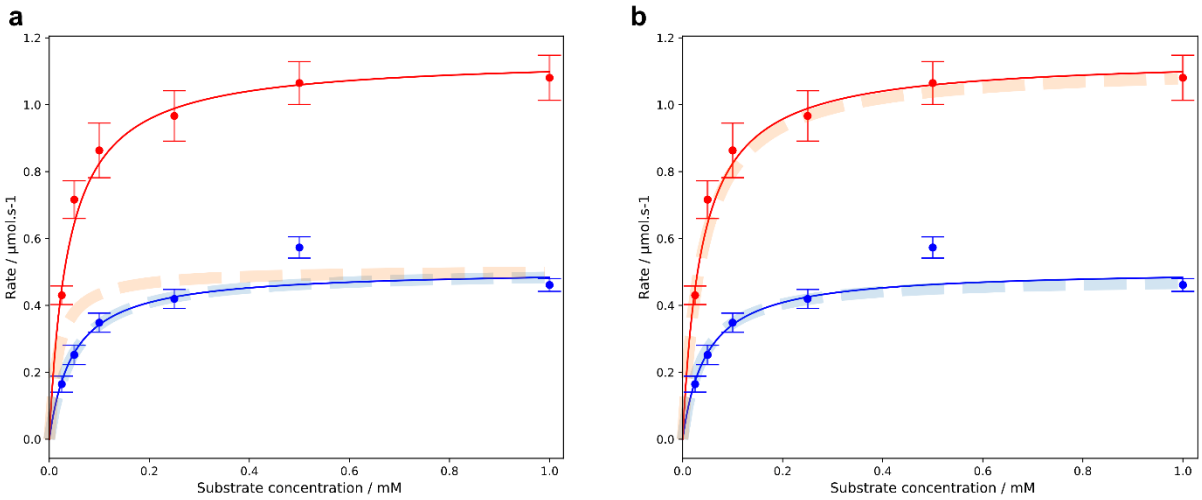

Figure S5: a) graph showing the experimental data (solid lines, arPTE blue, [arPTE][S^+][S^-] red) compared to the theoretical data (dashed transparent lines, same respective colours) of if the rate of k_1 (substrate on rate) is increased. The theoretical data with the increased k1 (red) does not match the experimental data of [arPTE][S^+][S^-]. B) A graph showing the experimental data compared to the theoretical data with an increased k_2 (rate of product release). Increasing the rate of product release for the theoretical data results in a curve that is in close agreement with the experimental data.

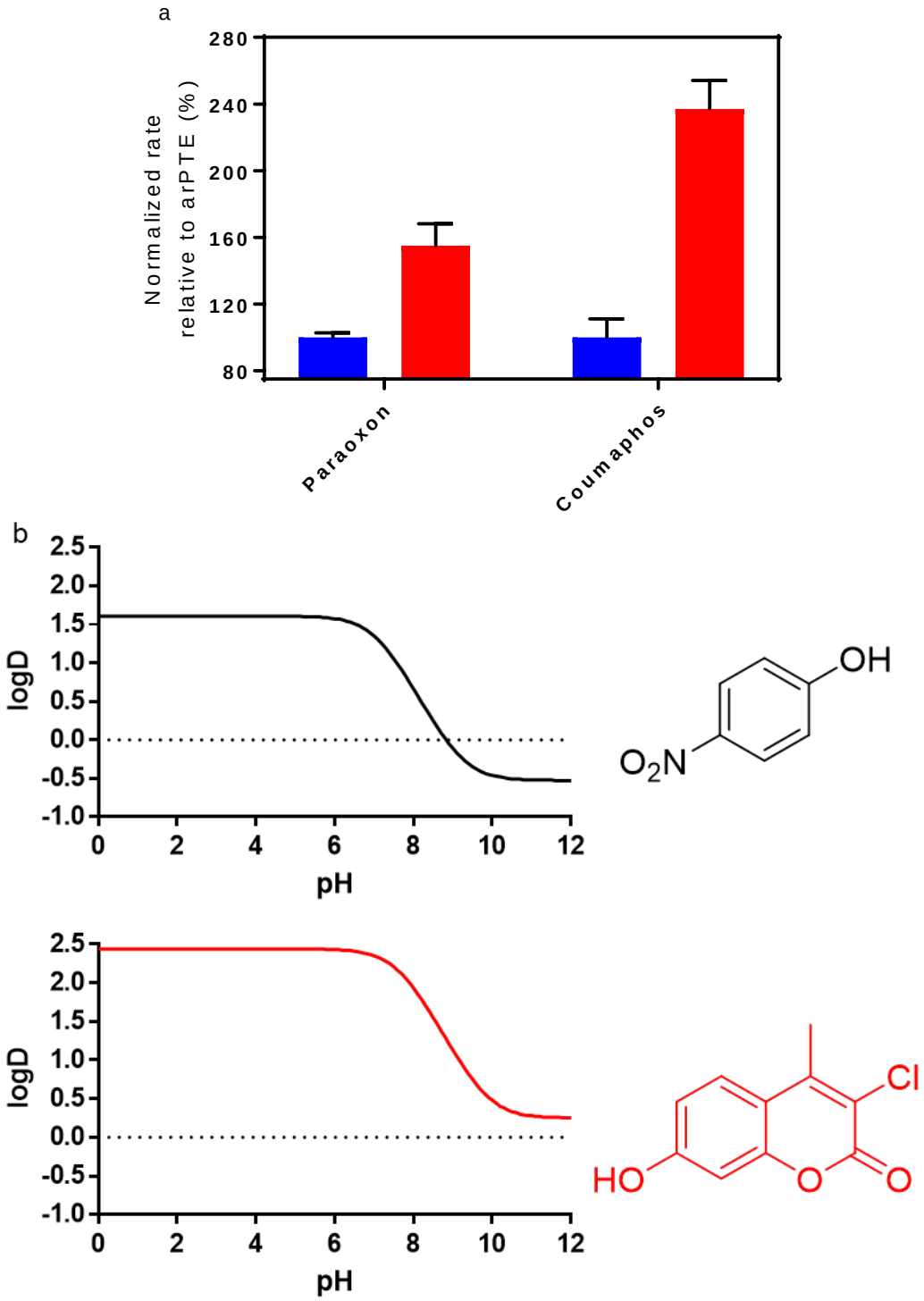

Figure S6: a) Comparison between the relative enhancement in rate for arPTE (blue) and [arPTE][S^+][S^-] (red) for the substrate paraoxon and the substrate coumaphos, for a same-batch preparation of the enzyme. The assay was done using 500 µM of substrate, a concentration where both paraoxon and coumaphos should be degraded at approximately the V_{max} rate. The activity of the enzyme for coumaphos hydrolysis to chlorferone was monitored through fluorescence at 460 nm. b) The logD of 4-nitrophenol (from paraoxon, black) and chlorferone (from coumaphos, red) as a function of pH. At pH 8.0 (assay condition) we see that both products would partition preferentially into a hydrophobic environment, and that chloreferone has significantly more hydrophobic character. Properties of these products were calculated using the ChemAxon Chemicalize software.(*6*)

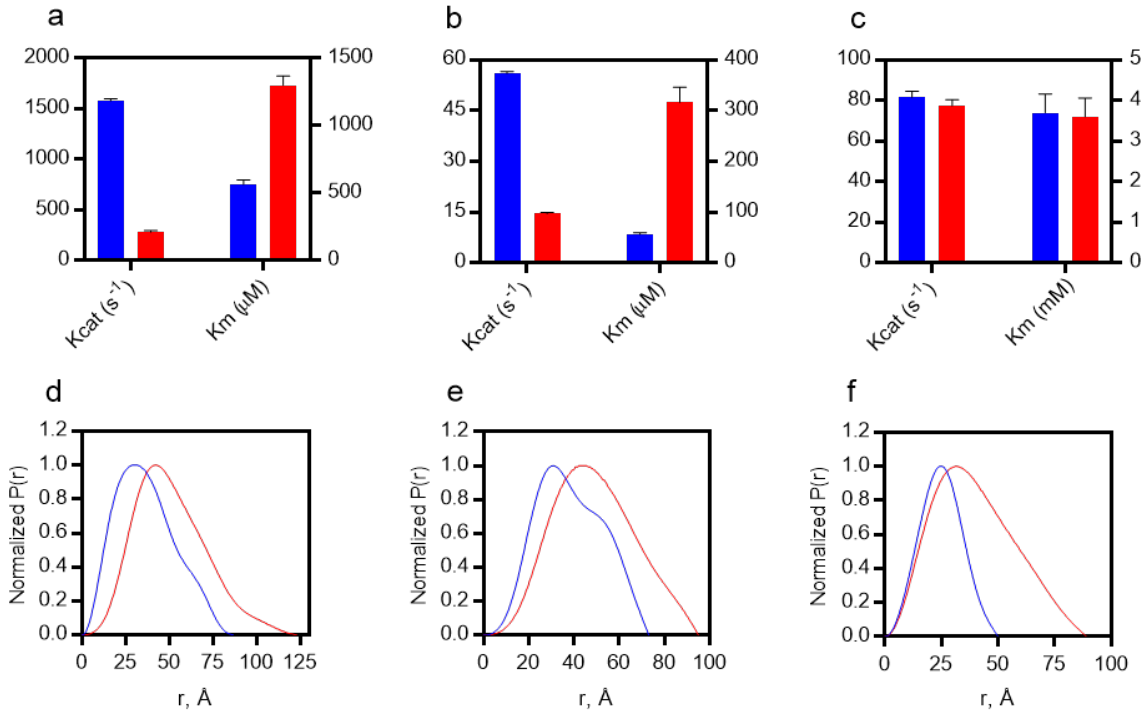

Figure S7: a) Activity of pdPTE-C23 (blue), a relative of arPTE, on paraoxon. [pdPTE-C23][S^+][S^-] (red) shows a decrease in the catalytic rate and an increase in K_m indicating lower affinity. b) Activity of αEst7 (blue) on paraoxon, with the [αEst7][S^+][S^-] (red) showing a decrease in activity and a decrease in affinity (higher K_m), consistent with inhibition of the active site. c) For the hydrolysis of DFP, DFPase (blue) and the [DFPase][S^+][S^-] (blue) shows no increase or decrease in kinetic parameters as a result of the surfactant conjugation. d) SAXS P(r) plot of pdPTE-C23 (blue) showing a similar profile of an increase in the R_g as arPTE after conjugation (red). e) SAXS P(r) plot of αEst7 (blue), again demonstrating an increased average radius upon conjugation (red). f) SAXS P(r) of DFPase (blue) also showing an average increase in radius from conjugation (red).

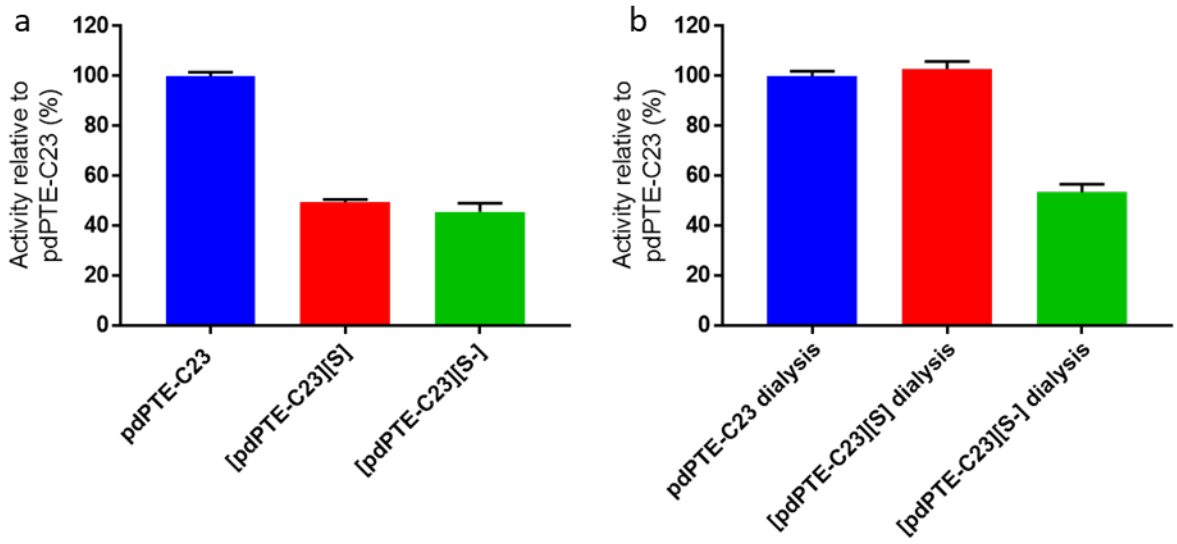

Figure S8: a) the activity of pdPTE-C23 for paraoxon is decreased when assayed in the presence of uncharged surfactant (1% w/v, IGEPAL-890 unoxidized, [pdPTE-C23][S]) and is similarly decreased in the presence of the charged surfactant (1% w/v, oxidized IGEPAL-890, [pdPTE-C23][S^-]). b) Assays after dialysis of these enzymes shows restoration of the paraoxon hydrolysis activity for [pdPTE-C23][S], but not for [pdPTE-C23][S^-]. This shows that the surfactant is inhibiting the active site, and that the charged surfactant remains associated with the enzyme even at the dilute concentrations used for the assay conditions. All assays were performed as described in the experimental section with the variations described above.

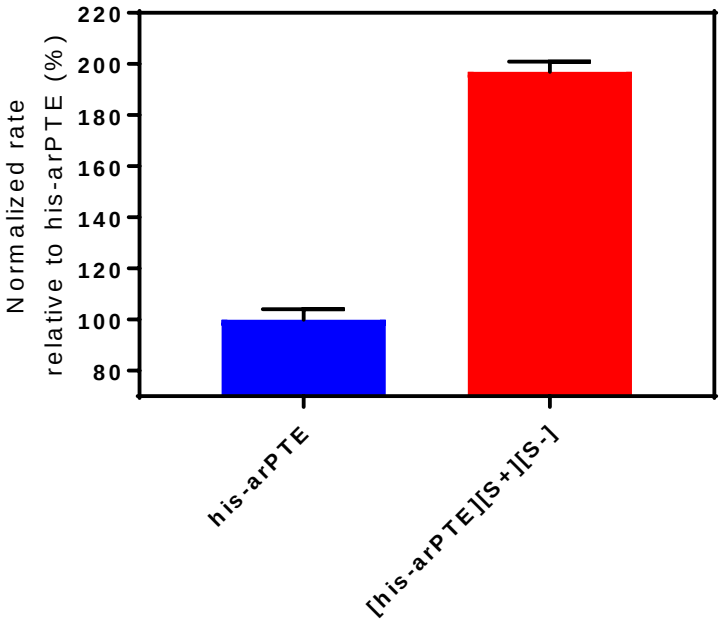

Figure S9: The comparison between the relative activity between his-tagged arPTE and his-tagged [arPTE][S^+][S^-]. The presence of the his-tag does not impede the ability of the surfactant corona to enhance the activity of arPTE.

3. Supplementary tables

Supplementary table 1. The parameters from SR-SAXS for the different enzymes and the corresponding bioconjugates.

	R_g (Å)	***r_{ave} (Å)***	***d_{max} (Å)***	***Porod exponent***
arPTE	28.2	36.2	90	3.8
[arPTE][S^+][S^-]	37.5	48.8	112	3.5
pdPTE-C23	28.4	36.5	87	3.5
[pdPTE-C23][S^+][S^-]	38.9	51.0	123	3.1
αEst7*	28.6	37.5	73	3.1
[αEst7][S^+][S^-]*	36.8	49	95	3.0
DFPase	18.7	24.9	50	3.7
[DFPase][S^+][S^-]	30.6	39.6	89	2.9

All parameters shown were determined using the scatter3 software analysis of the fitted data. All tested enzymes had an increase to the radius of gyration (R_g, realspace), radial average (r_{ave}), and maximum diameter (d_{max}). *αEst7 exists as a mixture of monomer and higher state oligomers (dimer, tetramer),(*7*) the data for αEst7 was fitted from that obtained by SEC-SR-SAXS, while the [αEst7][S^+][S^-] data was fit under the assumption that the bioconjugate behaves as a monomer, but it should be stated that in reality the bioconjugate would have some higher order oligomers present.

4. References

(1) Armstrong, J. P. K., Shakur, R., Horne, J. P., Dickinson, S. C., Armstrong, C. T., Lau, K., Kadiwala, J., Lowe, R., Seddon, A., Mann, S.*, et al.* (2015) Artificial membrane-binding proteins stimulate oxygenation of stem cells during engineering of large cartilage tissue. *Nat. Commun. 6*, 7405.

(2) Basham, M., Filik, J., Wharmby, M. T., Chang, P. C., El Kassaby, B., Gerring, M., Aishima, J., Levik, K., Pulford, B. C., Sikharulidze, I.*, et al.* (2015) Data Analysis WorkbeNch (DAWN). *J. Synchrotron Radiat. 22*, 853-8.

(3) Franke, D., Petoukhov, M. V., Konarev, P. V., Panjkovich, A., Tuukkanen, A., Mertens, H. D. T., Kikhney, A. G., Hajizadeh, N. R., Franklin, J. M., Jeffries, C. M.*, et al.* (2017) ATSAS 2.8: a comprehensive data analysis suite for small-angle scattering from macromolecular solutions. *J. Appl. Crystallogr. 50*, 1212-1225.

(4) Rambo, R. P. (2019) ScÅtter. *(Available at http://www.bioisis.net/tutorial/9)*.

(5) Breger, J. C., Ancona, M. G., Walper, S. A., Oh, E., Susumu, K., Stewart, M. H., Deschamps, J. R., and Medintz, I. L. (2015) Understanding How Nanoparticle Attachment Enhances Phosphotriesterase Kinetic Efficiency. *ACS Nano 9*, 8491-503.

(6) Swain, M. (2012) chemicalize.org. *J. Chem. Inf. Model. 52*, 613-615.

(7) Fraser, N. J., Liu, J. W., Mabbitt, P. D., Correy, G. J., Coppin, C. W., Lethier, M., Perugini, M. A., Murphy, J. M., Oakeshott, J. G., Weik, M.*, et al.* (2016) Evolution of Protein Quaternary Structure in Response to Selective Pressure for Increased Thermostability. *J. Mol. Biol. 428*, 2359-2371.